

Data driven isospin analysis of timelike octet baryons electromagnetic form factors and charmonium decay into baryon-anti-baryon

Jian-Ping Dai,^{1,*} Xu Cao,^{2,3,4,†} and Horst Lenske^{5,‡}

¹*Department of Physics, Yunnan University, Kunming 650091, China*

²*Institute of Modern Physics, Chinese Academy of Sciences, Lanzhou 730000, China*

³*University of Chinese Academy of Sciences, Beijing 100049, China*

⁴*Research Center for Hadron and CSR Physics, Lanzhou University and Institute of Modern Physics of CAS, Lanzhou 730000, China*

⁵*Institut für Theoretische Physik, Universität Giessen, D-35392 Giessen, Germany*

(Dated: April 12, 2023)

Inspired by the recent precise data, we perform model-independently an isospin decomposition of the timelike octet baryons electromagnetic form factors. As noted in our previous work, the relative magnitude of isoscalar and isovector component is determined with the input of data on various isospin channels. Herein we further assert that their relative phase can be constraint by the phase difference of oscillatory modulation of effective form factors between isospin channels. The framework is extended to analyze the data of differential cross sections and applied to the form factors of nucleon and hyperons with detail and isospin non-conservation of charmonium decay into baryon-anti-baryon as well. We address that isospin analysis is meaningful when the isospin broken scale is compared to or smaller than the uncertainties of data.

I. INTRODUCTION

As the lightest baryons, nucleons account essentially for all of the observable matter in the universe. However, since their non-pointlike nature was discovered more than sixty years ago [1], nucleon properties, e.g. the spin and radii, are still a puzzle, whose final solution is pending [2–5]. Moreover, understanding the structure of nucleons is of high importance for the physics of the whole set of baryons forming the lowest SU(3) octet. On an astrophysical scale, hyperons with a strange quark content, are expected to play a key role to understand the masses and sizes of compact object like neutron stars [6]. Electromagnetic form factors (EMFFs) are fundamental observables of baryons that are closely related to their static and dynamical properties [7, 8]. The transition amplitude of electron-positron annihilation into baryon-anti-baryon (or *vice versa*) is given by timelike EMFFs, which are complex and connected with the spacelike EMFFs by the dispersion relation [9]. The known sources of the imaginary part of amplitudes are multi-meson rescattering loops and intermediate vector meson excitations. While the former are incorporated by the dispersion analysis of the nucleon EMFFs including meson continua [9–11], the latter are only phenomenologically investigated in the isoscalar and isovector form factor [12].

In view of the precise data measured by several collaborations [13–16], it is timely to perform a data driven analysis based on the isospin decomposition. Though isospin conservation is given only approximately, the analysis is model-independent by its own provided that isospin mix-

ing is allowed. Isospin decomposition is in fact far from trivial when isoscalar and isovector components are both involved into $e^+e^- \rightarrow B\bar{B}$ reactions. At first glimpse, if one measures all the isospin channels, the isospin assignment of contributing vector meson above $B\bar{B}$ threshold shall be unambiguously determined. However, the isospin assignment of a light-quark meson or charmonium state is in fact highly non-trivial when both isoscalar and isovector components are populated in e^+e^- reactions. Take $N\bar{N}$ production as an example, two complex isospin amplitudes with at least three parameters (two moduli and one relative phase) are present but only two channels ($p\bar{p}$ and $n\bar{n}$) of mixed isospin ($I=0, 1$) are allowed. As a result, one can only constrain the range of two parameters, namely relative magnitude and relative phase if total cross sections (or equivalently effective form factors) are measured. It is further noted that complex electric and magnetic form factors are involved in the analysis of angular distribution and polarization observables. As a result, one cannot fully decompose all complex amplitudes, even if all observables were measured.

Following exactly the same argument, the isospin assignment of involved vector mesons cannot be determined in principle. Note that experimentally one knows the isospin of J/ψ and other 1^{--} pieces of charmonium not from their production in e^+e^- annihilation, but from their strongly suppressed isovector decays and the absence of charged partners. This is totally different from the case of γN or $\pi N \rightarrow \pi N$ reactions [17], where the full set of isospin channels is available to disentangle explicitly two isospin amplitudes $I = 1/2$ and $3/2$. A good example is $\rho(2150)$ and $\phi(2175)$, whose masses and widths with big uncertainties are overlapping. When only one of them is contributing and another one is forbidden by isospin conservation, the issue on isospin is obvious by itself. For instance, only $\rho(2150)$ is present in K^+K^-

* daijianping@ynu.edu.cn

† caoxu@impcas.ac.cn

‡ horst.lenske@physik.uni-giessen.de

spectrum of $e^+e^- \rightarrow J/\psi \rightarrow K^+K^-\pi^0$ [18], while only $\phi(2175)$ in $e^+e^- \rightarrow \phi\pi^+\pi^-$ [19]. However, the broad peak around 2.0 ~ 2.2 GeV clearly observed both in $e^+e^- \rightarrow K^+K^-$ [20] and $e^+e^- \rightarrow K^+K^-\pi^0\pi^0$ [21], would be from $\rho(2150)$ or $\phi(2175)$ or both, because the isospin of this peak is never determined. The $\omega(2290)$ with higher mass, solely contributing to $e^+e^- \rightarrow \omega\pi^0\pi^0$ [22], is also possibly contributing through interference considering its broad width. Under these circumstances, both $\rho(2150)$ and $\phi(2175)$ are probably contributing into these channels and their isospin cannot unambiguously be disentangled by their own.

In a word, isospin assignment of the involved vector mesons in $e^+e^- \rightarrow B\bar{B}$ cannot be determined from the $B\bar{B}$ data alone, except the special case of a Λ hyperon. More uncomfortably, in comparison with K^+K^- and $K^+K^-\pi^0\pi^0$ channels, the broad structure of $N\bar{N}$ spectra shows a global oscillation pattern [23–25] rather than resonant Breit-Wigner structures which resulted into the long confusion about their underlying mechanism. The proposed interpretations ranged from effects induced by the nucleon internal structure [23, 26], vector meson excitations [27–29], threshold opening [29], or final state interactions [30, 31]. In our previous paper we clarified the case on nucleon by introducing an isospin formalism allowing to decompose the amplitudes and cross sections [32], thus paving the way to a data driven isospin analysis of the continuum (dipole) component containing nucleon structure in timelike region as detailed in Sec. II. An extension to octet baryons is obvious and will be done in Sec. III. The whole framework is easily extended to analyze the isospin non-conservation of charmonium decay into baryon-anti-baryon in Sec. IV.

II. ABOUT NUCLEONS

The basics on the observables of $B\bar{B}$ production are shown in the Appendix A, following the usual definition in the literature. The effective nucleon form factor $|G_{\text{eff}}^N|$ shows an oscillating behavior around a smooth component $G_N^D(q^2)$,

$$|G_{\text{eff}}^N| = |G_N^D(q^2)| + G_N^{\text{osc}}(q^2), \quad (1)$$

$$|G_N^D(q^2)| = \frac{\mathcal{A}_N}{(1 + \frac{q^2}{m_a^2})(1 - \frac{q^2}{0.71(\text{GeV}^2)})^2}. \quad (2)$$

For protons ($N = p$), the dipole parameters for the normalization factor \mathcal{A}_p and the pole mass m_a^2 have been determined from the fit to the $|G_p|$ results from the BaBar experiment as $\mathcal{A}_p = 7.7$ and $m_a^2 = 14.8 \text{ GeV}^2$. The normalization for the neutron was obtained to be $\mathcal{A}_n = 4.87 \pm 0.09$ with the same pole mass as for the proton EFF [33].

The oscillatory structure G_N^{osc} is parameterized as [23],

$$G_N^{\text{osc}} = A_N \exp(-B_N p) \cos(C_N p + D_N), \quad (3)$$

with p being the nucleon momentum in the antinucleon rest frame. The normalization $A_N \ll \mathcal{A}_N$ is anticipated

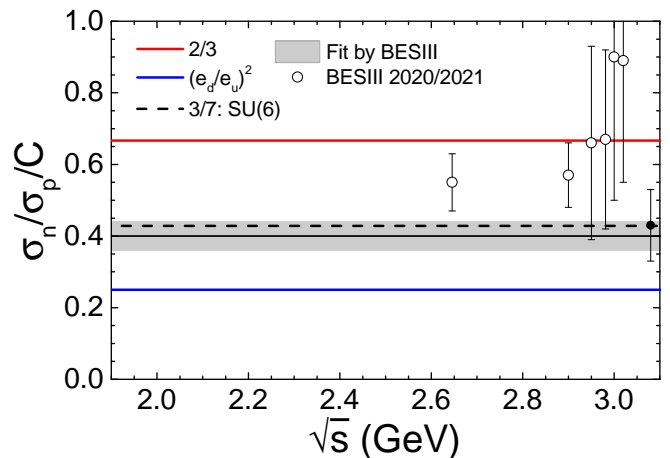


FIG. 1. (Color online) The cross section ratio of neutron to proton after subtracting the oscillation component and Coulomb correction. The BESIII data above 2.6 GeV are shown for comparison [33].

because no wide vector meson is found to couple strongly to $N\bar{N}$ below the charmonium region. However, a prominent hadronic counterexample is $e^+e^- \rightarrow \pi^+\pi^-$, where wide vector mesons, e.g. the ρ -meson, are strongly emergent. In order to keep G_N^{osc}/G_N^D small over a wide energy range the damping strength shall be strong enough, e.g. $B_N \gtrsim 0.5 \text{ GeV}^{-1}$. The momentum frequency shall be in a moderate range, $2 \lesssim C_N \lesssim 10 \text{ GeV}^{-1}$. Otherwise it will over-fit the data with artificial narrow structures when frequency is chosen too small ($C_N > 10 \text{ GeV}^{-1}$), or it contains too wide continuum which can be absorbed into the smooth component when the frequency is too large ($C_N < 2 \text{ GeV}^{-1}$). The fit to proton data in various schemes does follow these expectations [25, 33]. The neutron data of DM2 [34], FENICE [35], however, suffer from a limited energy range and low statistics. The near threshold SND data [36–38] are more involved the final state interaction, which need to be careful considered [30, 31]. The residual component is found to be $A_p = 0.07 \pm 0.01$ and $A_n = 0.08 \pm 0.03$ with universal parameters for proton and neutron [33]: $B_N = 1.01 \pm 0.24 \text{ GeV}^{-1}$, $C_N = 5.28 \pm 0.36 \text{ GeV}^{-1}$. The phases are $D_p = 0.31 \pm 0.17$ and $D_n = -3.77 \pm 0.55$, resulting into a relative phase for the proton and neutron oscillation being $\Delta\phi = (125 \pm 12)^\circ$.

As argued in our previous work [32], such oscillatory structures are the natural consequence of an interference between a leading component from nucleon structure and a residual amplitude from vector meson production above threshold. Thus, a ratio containing no oscillation is suggested,

$$\frac{\sigma_n^D}{\sigma_p^D/C} = \left| \frac{G_n^D}{G_p^D} \right|^2 = 0.40 \pm 0.03 \quad (4)$$

surprisingly a constant, albeit within uncertainties, over a wide range of energies. In Fig. 1, this constant is com-

pared to several values predicted for the spacelike region, namely the 3/7, a prediction of SU(6) symmetric nucleon wave function [39], together with the naive $e_u^2/e_d^2=1/4$ from the quark charge ratio [40] and 2/3 obtained from the values in constituent quark model [39]. It is also consistent with 0.4~0.5 predicted by QCD sum rule [40] and $(\mu_n/\mu_p)^2$ deduced from the asymptotic behaviour [41]. A recent theoretical analysis of the MARATHON experiment [42] finds quite-close values [43–45].

For a long time, there was barely any information on vector mesons above 2.6 GeV [46, 47]. In Fig. 1, the deviation of BESIII data from the constant in this energy range [33] shall be interpreted as the possible resonances with larger mass. The bold point just below the J/ψ mass peak is not supposed to become contaminated with light flavor vector mesons. Within the (large) error bars it is actually consistent with our postulation. This further supports our argument that the oscillation part G_N^{osc} is probably connected to vector meson excitation while the leading component G_N^D is what is actually related directly to the nucleon structure. In terms of the $|I, I_3\rangle = |0, 0\rangle$ and $|1, 0\rangle$ isospin components, this leading part is decomposed into the isoscalar (I_0) and isovector (I_1) amplitudes with regard to isospin symmetry [48]:

$$G_{p,n}^D = \frac{I_1^D \pm I_0^D}{\sqrt{2}}, \quad (5)$$

where the upper (lower) sign corresponds to the proton (neutron) case. The two isospin amplitudes are related by $I_1^D = I_0^D \delta_I e^{i\phi_I}$, rendering an isospin relevant ratio [32]:

$$R_I^{\text{eff}} = \frac{|G_p^D|^2 - |G_n^D|^2}{|G_p^D|^2 + |G_n^D|^2} = \frac{2\delta_I \cos \phi_I}{1 + \delta_I^2} = 0.43 \pm 0.03, \quad (6)$$

which constrains the range of δ_I and ϕ_I within an blue egg-shaped diagram as shown in Fig. 2. Considering that at leading order of $G_N^{osc}/|G_N^D| \ll 1$ [32],

$$G_N^{\text{osc}} \simeq \frac{|I_N^{\text{BW}}|}{\sqrt{2}} \cos(\phi_N^D - \phi_N^{\text{BW}}) + \frac{1}{4} \frac{|I_N^{\text{BW}}|^2}{G_N^D} \sin^2(\phi_N^D - \phi_N^{\text{BW}}) \quad (7)$$

is an equivalent of Eq. (3) regardless of next-to-leading order (NLO) contribution in the second line. Moreover, another significant result of our present work was to identify that the phase shift $\phi_p^{\text{BW}} = \phi_n^{\text{BW}}$ of Breit-Wigner (BW) distribution serves as a measure of the relative phase for the proton and neutron oscillation:

$$|\Delta\phi| = |D_n - D_p| = \arg \frac{I_1^D - I_0^D}{I_1 + I_0}, \quad (8)$$

thus constraining further the compatible values of δ_I and ϕ_I to rather well defined regions as indicated in the red correlation diagram displayed in Fig. 2. Interestingly, both $|I_0| = |I_1|$ and the in-phase scenario $\phi_I = 0$ are excluded with high statistical significance.

Assuming the isospin (or charge) symmetry $G_{E,M}^{u/n} = G_{E,M}^{d/p}$ and $G_{E,M}^{d/n} = G_{E,M}^{u/p}$, the isospin relation is a realization of the flavor decomposition of nucleon EMFFs [49],

$$G_{E,M}^p = \frac{2}{3} G_{E,M}^u - \frac{1}{3} G_{E,M}^d = \frac{1}{2} \left(\frac{G_{E,M}^{u+d}}{3} + G_{E,M}^{u-d} \right) \quad (9)$$

$$G_{E,M}^n = \frac{2}{3} G_{E,M}^d - \frac{1}{3} G_{E,M}^u = \frac{1}{2} \left(\frac{G_{E,M}^{u+d}}{3} - G_{E,M}^{u-d} \right) \quad (10)$$

which can be extracted via:

$$|\frac{G_M^{u+d}}{3}|^2 + |G_M^{u-d}|^2 = 2(2\tau + 1) \left(\frac{|G_p^D|^2}{2\tau + R_p^2} + \frac{|G_n^D|^2}{2\tau + R_n^2} \right) \quad (11)$$

$$\Re[\frac{G_M^{u+d}}{3} G_M^{u-d}] = (2\tau + 1) \left(\frac{|G_p^D|^2}{2\tau + R_p^2} - \frac{|G_n^D|^2}{2\tau + R_n^2} \right) \quad (12)$$

$$|\frac{G_E^{u+d}}{3}|^2 + |G_E^{u-d}|^2 = 2(2\tau + 1) \left(\frac{R_p^2 |G_p^D|^2}{2\tau + R_p^2} + \frac{R_n^2 |G_n^D|^2}{2\tau + R_n^2} \right) \quad (13)$$

$$\Re[\frac{G_E^{u+d}}{3} G_E^{u-d}] = (2\tau + 1) \left(\frac{R_p^2 |G_p^D|^2}{2\tau + R_p^2} - \frac{R_n^2 |G_n^D|^2}{2\tau + R_n^2} \right) \quad (14)$$

if the total cross section and the angular distribution are both measured. Therefore one cannot fully separate all EMFFs in the isospin basis if only the data of total and differential cross sections are available. The appendix A shows that this separation is attainable after including further two single-spin observables sensitive to $\Im(G_M G_E^*)$ and $\Re(G_M G_E^*)$, respectively. Without loss of generality one may use

$$\frac{G_M^{u+d}}{3} = G_M^{u-d} \delta_M e^{i\phi_M}, \quad \frac{G_E^{u+d}}{3} = G_E^{u-d} \delta_E e^{i\phi_E}. \quad (15)$$

With a parameterization of R_N :

$$R_N = \frac{r_N}{r_N + (\sqrt{q^2} - 2m_N)^2} \quad (16)$$

one finds $r_p = 3 \pm 2 \text{ GeV}^2$ and $r_n = 6 \pm 21 \text{ GeV}^2$ extracted from the proton data [25] and the neutron data [50], respectively. Then we could derive the following quantities from Eqs. (11,12) and Eqs. (13,14), respectively

$$R_I^M = \frac{2\delta_M \cos \phi_M}{1 + \delta_M^2}, \quad (17)$$

$$R_I^E = \frac{2\delta_E \cos \phi_E}{1 + \delta_E^2} \quad (18)$$

as a function of $\sqrt{q^2}$ in Fig. 3. If $R_p = R_n$, these ratios are identical to Eq. (6) as shown by the black line in Fig. 3. Thus, the interference between the isoscalar and isovector EMFFs is observed for the first time, though suffering from big uncertainties.

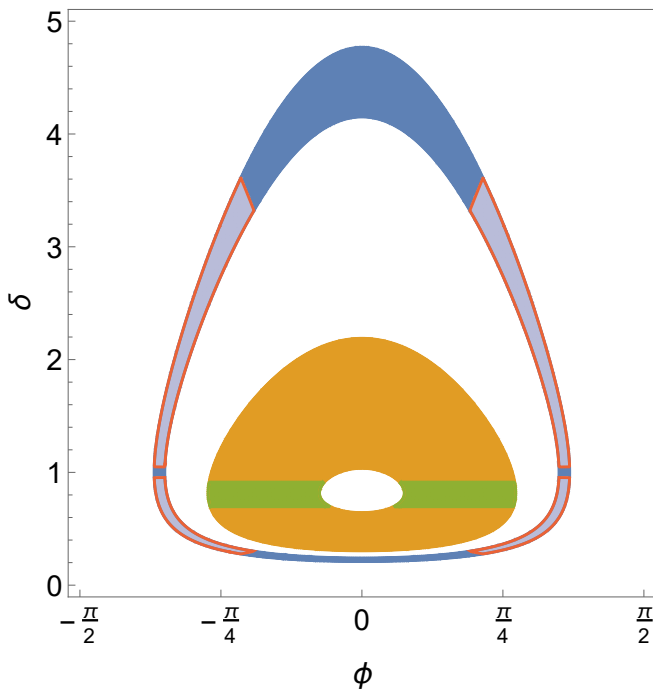


FIG. 2. (Color online) Permeable boundaries of relative magnitude δ and phase ϕ (see Eqs. (6, 8) for nucleon (outer region) and Σ (inner region), respectively).

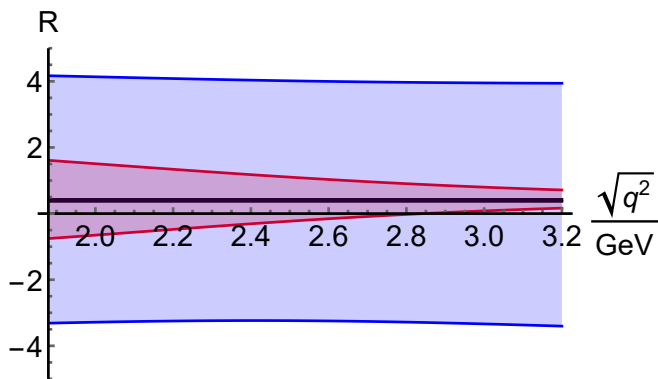


FIG. 3. (Color online) The R_T^M (red region) and R_T^E (blue region) extracted from data. When $R_p = R_n$ they both return back to the black line.

III. ABOUT HYPERONS

Many models constructed for nucleons in the timelike region have been extended to the whole octet for investigations of hyperon EMFFs. The region close to the reaction threshold is especially interesting considering the role of final-state interaction, as clearly indicated by an effective optical potential [51]. A high quality description of both proton and neutron EMFFs has been achieved by utilizing $N\bar{N}$ potential models that have been constructed within chiral effective field theory [30], phenomenological Jülich potential [52], and dispersion-theoretical analysis [10]. An extension to hyperon in

the timelike region is successful within the same frameworks [11, 53]. The properties of these form factors are significantly influenced by the final state interaction even at higher energies [31]. The hyperon EMFFs are also investigated within a covariant quark model [54, 55] and vector meson dominant (VMD) model [56–58]. A unified view is achieved within big uncertainties if comparing the timelike result to those in spacelike region calculated by chiral perturbation theory [59], light-cone sum rule [60, 61], basis light-front quantization [62–64], and Lattice QCD [65]. The role of sea quark contributions to the EMFFs of Σ hyperons is addressed within nonlocal chiral effective theory [66].

a. Hyperons with Strangeness $S=-1$ The striking oscillation phenomenon has not been confirmed for hyperons mainly limited by the data accuracy at hand, though attempts were made in literature [67, 68]. However, the precision of data is sufficient for an isospin analysis in line with the spirit in Sec. II and also of U-spin considerations [34, 69]. The $\Sigma\bar{\Sigma}$ system is of three isospin components I_0 , I_1 , and I_2 , but the $e^+e^- \rightarrow \Sigma\bar{\Sigma}$ reaction populates only the isoscalar and isovector amplitudes I_0 and I_1 . The corresponding isospin decomposition of Σ^+ , Σ^- and Σ^0 is [70]

$$G_+ = \frac{1}{\sqrt{2}}I_1 + \frac{1}{\sqrt{3}}I_0 \quad (19)$$

$$G_- = \frac{1}{\sqrt{2}}I_1 - \frac{1}{\sqrt{3}}I_0 \quad (20)$$

$$G_0 = \frac{1}{\sqrt{3}}I_0 \quad (21)$$

Hence if $G_{\pm,0}$ are measured, both isospin amplitudes can be determined in principle from the sum and the difference where the parameterizations $G_{\pm,0} = |G_{\pm,0}|e^{i\phi_{\pm,0}}$ are to be used. Neglecting the small mass difference within the Σ isospin triplet, a bound for the EMFF of the neutral channel is deduced:

$$4|G_0|^2 = |G_+|^2 + |G_-|^2 - 2|G_+||G_-|\cos(\phi_+ - \phi_-) \quad (22)$$

leading to a model independent bound in a compact form:

$$||G_+| - |G_-|| \leq 2|G_0| \leq |G_+| + |G_-| \quad (23)$$

This puts forward a constraint to Σ^0 EFF (and therefore cross section), see Fig. 4. Here we use the parameterization of EFF from BESIII [71, 72] instead of a dipole form in Eq. (2):

$$|G_{\text{eff}}^{\Sigma}| = \frac{c_0^{\Sigma}}{(s - c_1)^2(\pi^2 + \ln^2(s/\Lambda_{QCD}^2))} \quad (24)$$

with $c_1 = 1.95$, $c_0^{\Sigma^-} = 0.64$, and $c_0^{\Sigma^+} = 2.0$. Above bound is surprisingly narrower than the errors of BaBar [73] and Belle [74]. As seen in Fig. 4, the bound of Eq. (23) complies surprisingly well with the BESIII data [72]. The good agreement is even clearer in the plot of the EFF ratios of Σ^- to Σ^+ and Σ^0 to Σ^+ as shown in Fig. 5. The error of the predicted ratio between Σ^0 to Σ^+ (red band)

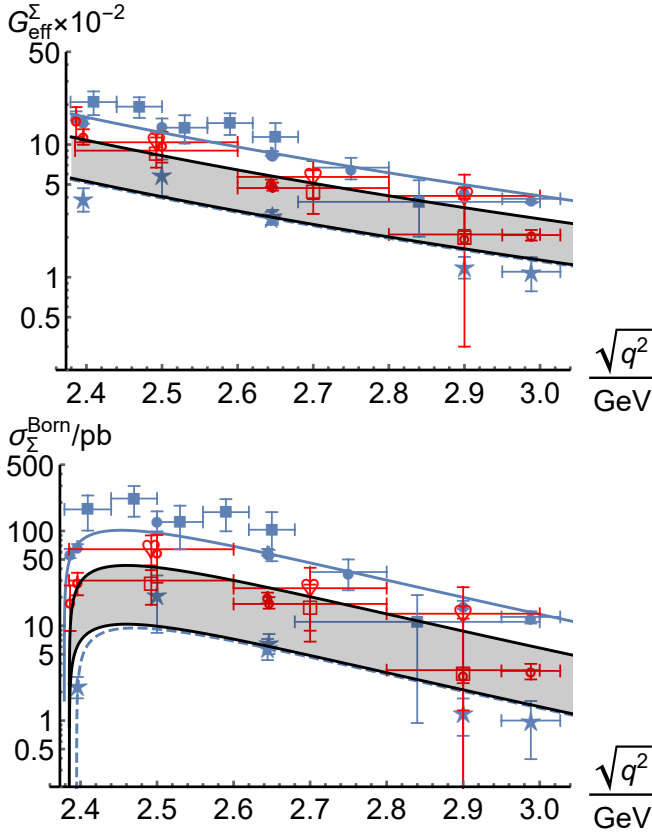


FIG. 4. (Color online) The EFF (upper panel) and cross section (lower panel) of Σ^\pm and Σ^0 . The dashed and solid line in blue are for Σ^- and Σ^+ , respectively. The solid star points in blue are data of Σ^- from BESIII [71]. The solid points are data of Σ^+ from Belle (blue square) [74] and BESIII (blue dot) [71]. The open red points are data of Σ^0 from BaBar (square) [73], Belle (heart) [74] and BESIII (dot) [72]. The grey bands are the predicted constraint of Σ^0 by Eq. (23).

is a bit worse than those extracted directly from data (grey band).

On the other hand, the same procedure as in Sec. II could be applied to extract the $I_{0,1}$ amplitudes from the EFFs of the charged members of the Σ isospin triplet. The cross section ratio of Σ^+ to Σ^- is extracted to be 9.7 ± 1.3 from recently BESIII data [71], translated to the blue band in Fig. 5. This results into

$$R_I^{\text{eff}} = \frac{|G_+|^2 - |G_-|^2}{|G_+|^2 + |G_-|^2} = \frac{2\sqrt{6}\delta_I \cos \phi_I}{3\delta_I^2 + 2} = 0.81 \pm 0.16 \quad (25)$$

which implies a larger interference term between I_1 and I_0 than that found for the nucleon doublet in Eq. (6). The bound of Eq. (25) is plotted as the inner orange egg-shaped region in Fig. 2, which is more tightly constrained than those of nucleon.

A closer inspection of Fig. 5 shows that the data are not fully consistent with a constant ratio but may contain an energy dependent variation. However, the precision of the data at present is insufficient for a finer exploration

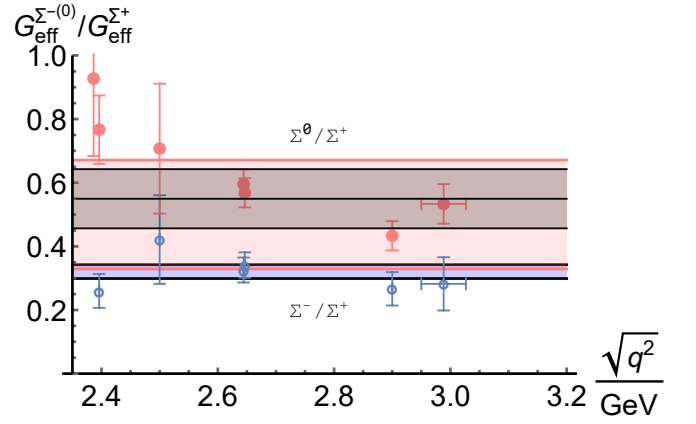


FIG. 5. (Color online) The EFF ratio of Σ^- to Σ^+ (blue band and points) is compared to that of Σ^0 to Σ^+ (red band and points). The blue and grey band are fitted to data by a constant. The red band is the predicted constraint by Eq. (23). The data are from BESIII [71, 72].

of possible oscillation structures [67]. So $G_{\pm,0}^D$ and $G_{\pm,0}$ are not distinguished further. As a consequence the information on ϕ_I can not be extracted from the relative phase for the Σ^+ and Σ^- oscillation. However, the measurement of Σ^0 channel supplies another constraint:

$$\frac{|G_0|^2}{|G_+|^2 + |G_-|^2} = \frac{1}{3\delta_I^2 + 2} = 0.27 \pm 0.04 \quad (26)$$

depicted by the grey band in Fig. 5. Then the allowed region of δ_I and ϕ_I is the grass green area in Fig. 2. The value $\delta_I = 1$ is excluded with high statistical significance. The in-phase $\phi_I = 0$ is firmly excluded. In the future these two methods could be used to cross-check the obtained constraint of the Σ isospin amplitudes or quantify even the violation of isospin symmetry if more precise data of EFF are available. Similar to Eq. (17) and Eq. (18), corresponding hyperon ratios R_+ and R_- are extracted from the data of angular distribution as well. The Σ^0 channel further separates the moduli of isoscalar and isovector EMFFs:

$$\left| \frac{G_M^0}{\sqrt{3}} \right|^2 = (2\tau + 1) \frac{|G_0|^2}{2\tau + R_0^2} \quad (27)$$

$$\left| \frac{G_M^1}{\sqrt{2}} \right|^2 = \frac{2\tau + 1}{2} \left(\frac{|G_+|^2}{2\tau + R_+^2} + \frac{|G_-|^2}{2\tau + R_-^2} - \frac{2|G_0|^2}{2\tau + R_0^2} \right) \quad (28)$$

$$\left| \frac{G_E^0}{\sqrt{3}} \right|^2 = (2\tau + 1) \frac{R_0^2 |G_0|^2}{2\tau + R_0^2} \quad (29)$$

$$\left| \frac{G_E^1}{\sqrt{2}} \right|^2 = \frac{2\tau + 1}{2} \left(\frac{R_+^2 |G_+|^2}{2\tau + R_+^2} + \frac{R_-^2 |G_-|^2}{2\tau + R_-^2} - \frac{2R_0^2 |G_0|^2}{2\tau + R_0^2} \right) \quad (30)$$

The numerical calculation is postponed because of lacking of the data. A rough R_+ is measured by BESIII and statistics are not sufficient to extract R_- and R_0 [71].

Assuming flavor symmetry $G_{E,M}^{u/\Sigma^+} = G_{E,M}^{d/\Sigma^-} = G_{E,M}^{u/\Sigma^0} = G_{E,M}^{d/\Sigma^0}$, the flavor decomposition of Σ isotriplet

is [65]

$$G_{E,M}^+ = -\frac{1}{3}G_{E,M}^s + \frac{2}{3}G_{E,M}^u \quad (31)$$

$$G_{E,M}^- = -\frac{1}{3}G_{E,M}^s - \frac{1}{3}G_{E,M}^d \quad (32)$$

$$G_{E,M}^0 = -\frac{1}{3}G_{E,M}^s \quad (33)$$

The ratio in Eq.(25) means that light up and down quarks contribute significantly to the Σ^\pm EMFFs.

A naive prediction from isoscalar diquark dominance is $G_\Lambda = -G_0$ [75], consistent with the data but within big errors [73, 76–79], anticipating, however, a significant violation of that relation. The ratios of Σ^0 to Λ EFFs and cross sections deviate obviously from a constant over the covered energy range as indicated by these data. The underlying reason, e.g. vector mesons above threshold or a violation of $G_\Lambda = -G_0$, is not yet known.

b. $S=-2$ Hyperons The cross section ratio between $e^+e^- \rightarrow \Xi^0\bar{\Xi}^0$ and $e^+e^- \rightarrow \Xi^-\bar{\Xi}^+$ [80–83] from BESIII below charmonium region is 1.25 ± 0.15 , consistent with 1.0 within 2σ . The isospin decomposition of $\Xi^{-,0}$ is the same with nucleon, see Eq. (5), resulting into

$$R_I^{\text{eff}} = \frac{|G_{\Xi^-}^D|^2 - |G_{\Xi^0}^D|^2}{|G_{\Xi^-}^D|^2 + |G_{\Xi^0}^D|^2} = 0.22 \pm 0.15, \quad (34)$$

This put a very loose constraint on the ratio of moduli δ , as shown in Fig. 6. Comparing to Fig. 2, the isospin components of nucleon, Σ and Ξ are explicitly distinguished by the present data. The data of R_{Ξ^0} and R_{Ξ^-} are yet unavailable.

Assuming flavor symmetry $G_{E,M}^{u/\Xi^-} = G_{E,M}^{d/\Xi^0}$, the quark flavor decomposition of Ξ isospin doublet is [65]

$$G_{E,M}^{\Xi^-} = -\frac{1}{3}G_{E,M}^s - \frac{1}{3}G_{E,M}^u \quad (35)$$

$$G_{E,M}^{\Xi^0} = -\frac{1}{3}G_{E,M}^s + \frac{2}{3}G_{E,M}^d \quad (36)$$

The nearly equivalent EFFs of $e^+e^- \rightarrow \Xi^-\bar{\Xi}^+$ and $\Xi^0\bar{\Xi}^0$ means that light up and down quarks contribute insignificant but the strange quarks are dominant in the EMFFs of Ξ hyperons.

IV. ABOUT CHARMONIUM DECAY

The isospin analysis analyses discussed in the previous sections are also applicable to the decay of Charmonium, which is the topic of this section. However, because of lack of data the discussion is of a more qualitative nature aiming at pointing out the perspectives of future experiments. Considering the emergence of the more and more precise data, the results presented below may be helpful to prepare experiments and to interpret the upcoming experimental results [94]. The Charmonium decay to $B\bar{B}$ is dominant by the isoscalar hadronic component with

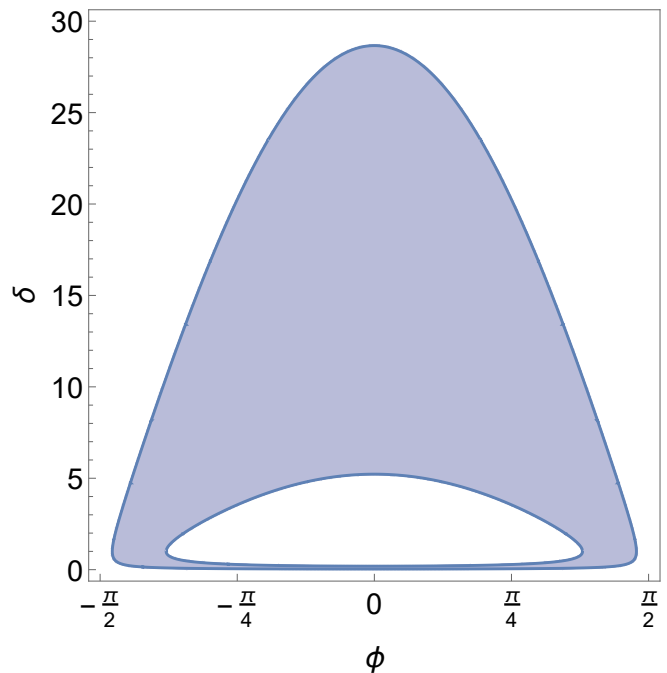


FIG. 6. (Color online) Permeable boundaries of relative magnitude δ and phase ϕ for Ξ baryon.

minor isospin violating a electromagnetic and a mixed strong-electromagnetic contributions [95].

The ratios R_I^{eff} , R_I^M , and R_I^E serve as the quantification of isospin non-conservation to the total, electric and magnetic contribution. As shown in Table I, the branching ratios of $J/\psi \rightarrow B\bar{B}$ in the same isospin multiplets are compatible within a relative accuracy of around 10% [85], resulting into nearly zero R_I^{eff} , thus reflecting the approximate isospin symmetry.

If including the information on the measured α_B , an important observation is that the isospin non-conservation mainly comes from the electric nucleonic decay amplitude and the magnetic Ξ amplitude. Remarkably, the isospin violating processes contribute potentially around 10% for $J/\psi \rightarrow N\bar{N}$, indicated both by branching ratios and α_B . The isospin non-conservation from decay to $\Xi\bar{\Xi}$ contributes potentially around 10%, attaining the same level between branching ratios and α_B of both J/ψ and $\psi(2S)$. The isospin violation part of electric amplitude of $\psi(2S) \rightarrow N\bar{N}$ and $\Sigma\bar{\Sigma}$ is of the same magnitude with the isospin conserving one. This is in sharp contrast with the level of isospin violation indicated in branching ratios, barely less than 10%.

The data on $J/\psi \rightarrow \Sigma^0\bar{\Sigma}^0$ and $J/\psi \rightarrow \Sigma^+\bar{\Sigma}^-$ is already measured. It is trivially to predict the values of $J/\psi \rightarrow \Sigma^-\bar{\Sigma}^+$ since they are equal to the other two channels under isospin conservation. The ratio of the branching ratios of $J/\psi \rightarrow \Sigma^0\bar{\Sigma}^0$ and $J/\psi \rightarrow \Sigma^+\bar{\Sigma}^-$ gives a very rough estimation for δ_I :

$$0.022 < \delta_I < 1.4 \quad (37)$$

TABLE I. The isospin non-conservation percentage R_I^{eff} , R_I^M , and R_I^E extracted from the branching ratios listed in Particle Data Group [84] and the measured α_B in literature.

Decay process	Branching ratio	α_B	R_I^{eff}	R_I^M	R_I^E
$J/\psi \rightarrow p\bar{p}$	$(2.120 \pm 0.029) \times 10^{-3}$	$0.595 \pm 0.012 \pm 0.015$ [85]	0.007 ± 0.039	0.02 ± 0.05	-0.11 ± 0.26
$J/\psi \rightarrow n\bar{n}$	$(2.09 \pm 0.16) \times 10^{-3}$	$0.50 \pm 0.04 \pm 0.21$ [85]			
$J/\psi \rightarrow \Xi^0 \bar{\Xi}^0$	$(1.17 \pm 0.04) \times 10^{-3}$	$0.66 \pm 0.03 \pm 0.05$ [86]	0.09 ± 0.04	0.10 ± 0.04	-0.01 ± 0.10
$J/\psi \rightarrow \Xi^- \bar{\Xi}^+$	$(0.97 \pm 0.08) \times 10^{-3}$	$0.586 \pm 0.012 \pm 0.010$ [87]			
$J/\psi \rightarrow \Sigma^0 \bar{\Sigma}^0$	$(1.172 \pm 0.032) \times 10^{-3}$	$-0.449 \pm 0.020 \pm 0.008$ [88]			
$J/\psi \rightarrow \Sigma^+ \bar{\Sigma}^-$	$(1.07 \pm 0.04) \times 10^{-3}$	$-0.508 \pm 0.006 \pm 0.004$ [89]			
$J/\psi \rightarrow \Sigma^- \bar{\Sigma}^+$	—	—			
$J/\psi \rightarrow \Lambda \bar{\Lambda}$	$(1.89 \pm 0.09) \times 10^{-3}$	$0.461 \pm 0.006 \pm 0.007$ [90]			
$J/\psi \rightarrow \Lambda \bar{\Sigma}^0 + \text{c.c.}$	$(2.83 \pm 0.23) \times 10^{-5}$	—			
$\psi(2S) \rightarrow p\bar{p}$	$(2.94 \pm 0.08) \times 10^{-4}$	$1.03 \pm 0.06 \pm 0.03$ [91]	-0.020 ± 0.028	0.02 ± 0.04	-1.0 ± 0.8
$\psi(2S) \rightarrow n\bar{n}$	$(3.06 \pm 0.15) \times 10^{-4}$	$0.68 \pm 0.12 \pm 0.11$ [91]			
$\psi(2S) \rightarrow \Xi^0 \bar{\Xi}^0$	$(2.3 \pm 0.4) \times 10^{-4}$	$0.65 \pm 0.09 \pm 0.14$ [86]	-0.11 ± 0.08	-0.12 ± 0.08	-0.04 ± 0.28
$\psi(2S) \rightarrow \Xi^- \bar{\Xi}^+$	$(2.87 \pm 0.11) \times 10^{-4}$	$0.693 \pm 0.048 \pm 0.049$ [92]			
$\psi(2S) \rightarrow \Sigma^0 \bar{\Sigma}^0$	$(2.35 \pm 0.09) \times 10^{-4}$	$0.71 \pm 0.11 \pm 0.04$ [88]			
$\psi(2S) \rightarrow \Sigma^+ \bar{\Sigma}^-$	$(2.43 \pm 0.10) \times 10^{-4}$	$0.682 \pm 0.03 \pm 0.011$ [89]	-0.074 ± 0.026	-0.12 ± 0.03	0.8 ± 0.4
$\psi(2S) \rightarrow \Sigma^- \bar{\Sigma}^+$	$(2.82 \pm 0.09) \times 10^{-4}$	$0.96 \pm 0.09 \pm 0.03$ [93]			
$\psi(2S) \rightarrow \Lambda \bar{\Lambda}$	$(3.81 \pm 0.13) \times 10^{-4}$	$0.82 \pm 0.08 \pm 0.02$ [88]			
$\psi(2S) \rightarrow \Lambda \bar{\Sigma}^0 + \text{c.c.}$	$(1.6 \pm 0.7) \times 10^{-6}$	—			

In analogy to the Eqs. (27,29) the ratio $R_0 = 2.11 \pm 0.07$ of $J/\psi \rightarrow \Sigma^0 \bar{\Sigma}^0$ channel is the relative modulus of isoscalar electric and magnetic amplitudes, to be compared to $R_0 = 0.64 \pm 0.13$ extracted from the data of $\psi(2S) \rightarrow \Sigma^0 \bar{\Sigma}^0$ Channel.

It is feasible to explore the magnitude of isospin non-conservation if all decay channels are measured. This is accessible for $\psi(2S) \rightarrow \Sigma \bar{\Sigma}$ as seen in Table I with the help of Eqs. (27,28,29,30):

$$\delta_I = 0.28 \pm 0.06, \phi_I = 88.1 \pm 0.7^\circ \text{ or } -91.9 \pm 0.7^\circ \quad (38)$$

$$\delta_M = 0.33 \pm 0.07, \phi_M = 78.2 \pm 1.0^\circ \text{ or } -101.8 \pm 1.0^\circ \quad (39)$$

$$\delta_E = 0.48 \pm 0.23, \phi_E = 65 \pm 15^\circ \text{ or } -115 \pm 15^\circ \quad (40)$$

resulting into the same conclusion above that the isospin violation part of electric amplitude of $\Sigma \bar{\Sigma}$ is potentially larger, however, yet at the same level with magnetic and total amplitudes if considering the big errors. This situation will probably be scrutinized in the future experiment considering the large error of α_B in $\psi(2S) \rightarrow \Sigma \bar{\Sigma}$. It is also concluded that isospin violation and conservation parts tend to be orthogonal.

The branching ratios of J/ψ and $\psi(2S) \rightarrow \Lambda \bar{\Lambda}$ are found to be around 1.6 times larger than that of $\Sigma^0 \bar{\Sigma}^0$, indicating a moderate breaking of isospin symmetry as expected. The same level of violation is observed for $\psi(3770)$ at CLEO-c Collaboration [96]. The branching

ratio of isospin violation decay J/ψ and $\psi(2S) \rightarrow \Lambda \bar{\Sigma}^0 + \text{c.c.}$ is around two orders in magnitude than that of the corresponding isospin allowed decays, hinting also to a small isospin violation in the decay width.

This scale of isospin violation is compatible with the analysis of SU(3) flavor symmetry [97] and a parameterization of effective amplitudes [98]. It is in the same level as the background from the continuum, e.g. contributions of baryon structure in Sec. II. If higher precision of measurement is feasible in future, it is definitely required to carefully examine the interference between charmonium and continuum amplitudes on the measurement of branching fractions and angular distributions [99]. For instance, it is anticipated that the the measured J/ψ line shape is distorted from a Breit-Wigner form by this interference term in $p\bar{p}$ and $n\bar{n}$ channels [97, 100]. Compared to the decay width, the angular distribution is more sensitive to the isospin violating part due to its interference with the much larger isospin conserving amplitude. A precise calculation of α_B would surely be helpful [101, 102] if higher order corrections are properly considered [103, 104].

The precision of broad Charmonium states above $D\bar{D}$ threshold is far from being adequate for the investigation of isospin violation contribution. In the near future more detailed measurement of the line shape of $\psi(3770)$ can be used to easily check our claim in Eq. (7). Fig. 7

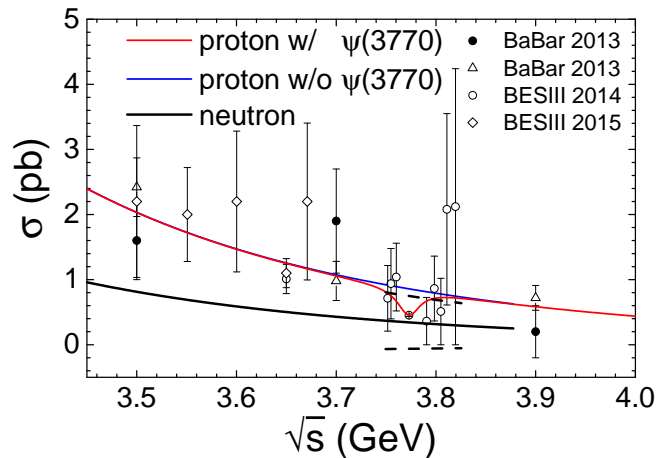


FIG. 7. (Color online) The cross sections of $e^+e^- \rightarrow p\bar{p}$ and $e^+e^- \rightarrow n\bar{n}$ in the vicinity of $\psi(3770)$. The blue and black line are dipole parameterization in Eq. (2). The red line is a coherent sum of Breit-Wigner form of $\psi(3770)$ with continuum dipole form in Eq. (2). The dashed line is the predicted peak position of $\psi(3770)$ in $e^+e^- \rightarrow n\bar{n}$. The data of $e^+e^- \rightarrow p\bar{p}$ are from BaBar [109, 110] and BESIII [111, 112].

shows the cross sections of $e^+e^- \rightarrow p\bar{p}$ and $e^+e^- \rightarrow n\bar{n}$ in the vicinity of $\psi(3770)$. The dip in the $e^+e^- \rightarrow p\bar{p}$ results from a destructive interference of $\psi(3770)$ and continuum. Considering the unknown $\Delta\phi = D_n - D_p$ in the charmonium region, a solid prediction can only be made by Eq. (7) to the range of peak or dip position of $\psi(3770)$ in $e^+e^- \rightarrow n\bar{n}$, as indicated by the dashed line. The upper line, e.g. a peak, is preferred for two reasons. First, the lower line extends into unphysical negative values. Second, the $\Delta\phi$ is expected to be weakly energy dependent and its value below 3.0 GeV favors a peak of $\psi(3770)$ in $e^+e^- \rightarrow n\bar{n}$. However, both reasons suffer from large errors so the dip shape of $\psi(3770)$ in $e^+e^- \rightarrow n\bar{n}$ is not fully excluded.

As can be seen in Fig. 7, the relative magnitude of $|I_N^{\text{BW}}/I_N^D|$ is around 0.3 for $\psi(3770)$ but around 0.1 \sim 0.2 for light mesons, both of which is in the same level of relative accuracy of local data. So the NLO contribution in Eq. (7) can not be identified by the currently available data. In other word, the data are well described both by the Breit-Wigner form and an oscillatory function, as demonstrated in detail in our previous work [32]. Hopefully the precision of data in the vicinity of $\psi(3770) \rightarrow p\bar{p}$ will approach to the same level with that below 3.0 GeV and validate the NLO contribution. Similar argument can be applied to $\psi(3770) \rightarrow \Lambda\bar{\Lambda}$ as well [78]. However, this is an extremely trivial phenomenon, already known from Flatté parametrizations or from a Fano line shape analysis of resonances, for instance, in the $\psi(3770) \rightarrow D\bar{D}$ reaction[105]. The underlying mechanism includes three-gluon and D -meson loop contributions [106–108].

V. SUMMARY AND CONCLUSION

Based on the isospin analyses, the periodic oscillation structures of nucleon effective form factors in the timelike region are attributed to manifestation of light unflavored vector mesons. The continuum dipole part of proton and neutron EFFs is used to determine the range of the relative phase and relative magnitude between isoscalar and isovector component of EFFs. We further point out that the relative phase is constrained by the phase difference between the oscillatory modulation of proton and neutron EFFs. The isospin analyses are extended to the angular distributions. Furthermore we successfully generalize the whole framework to the SU(3) octet baryons. An important result is that the range of the cross section of neutral Σ hyperon channel can be predicted from the measured cross section of charged Σ^\pm hyperon channel.

Isospin violation in the isovector form factors of the nucleon are predicted to be originated from strange EMFFs as calculated by LQCD [113] and by chiral perturbation theory [114]. At present the timelike $N\bar{N}$ data are not precise enough to explore these kind of contribution. Alternatively, we demonstrate that the precise data of J/ψ and $\psi(2S)$ decay allow for a first glimpse of the isospin non-conservation amplitudes within the same framework.

A better knowledge of the vector meson spectrum [115, 116] will certainly deepen our understanding of dipole part of the timelike nucleon EMFFs. Their interfering contributions induce the oscillation structures seen in the cross section data. A more dedicate study is required to go beyond the simple parameterization in Eq. (3). Though recently BESIII collaboration measured cross sections and invariant mass spectra of many channels with unprecedented accuracy, the properties of the vector mesons above $N\bar{N}$ threshold are still poorly understood. The proper description of the interference between amplitudes resulting from the decay into wide vector mesons and continuum process is a demanding task for theory, because e.g. a coupled-channel framework of multi-meson final states is by far too involved, if not impossible. As a result, phenomenological fits are inadequate to extract precisely the masses and widths of vector mesons from data. A complicated and time-consuming multi-channel partial wave analysis, possibly combined with a dispersion-theoretical framework, would be required to extract meson spectra for the available data. Unfortunately, the meson spectra above $N\bar{N}$ threshold is hardly accessible in the constituent quark model [46, 117–120]. Unquenched lattice QCD would be helpful but such calculations are yet unavailable.

In conclusion, even a full analysis of e^+e^- reactions does not allow by itself to determine the isospin of vector mesons, and input from theoretical side is indispensable. At present it is premature to claim the isospin of the local structures in $e^+e^- \rightarrow N\bar{N}$, but instead, it is safely to identify them as vector mesons rather than something else, as clearly illustrated in our paper. To bridge the seemingly small gap between two conclusions, plenty of ex-

perimental and theoretical efforts are required, a disappointing fact that has to be accepted. The isospin analyses in this paper give rise of another perspective providing that the isospin broken scale is comparable to or smaller than the uncertainties of data. With the help of available data, our analysis of isospin EFFs and EMFFs in the timelike region identified unambiguously the interference between them and unraveled the compatible range of parameters. The conclusions are robust to large extent in view of its model independence. So it paves the way for a fully consistent understanding of timelike and spacelike nucleon form factors. The proposed Super τ -Charm facility (STCF) [121] gives the opportunity to further scrutinize the scenario discussed here.

ACKNOWLEDGMENTS

This work is supported by the National Natural Science Foundation of China (Grants Nos. U2032109, 1216050075 and 12075289) and the Strategic Priority Research Program of Chinese Academy of Sciences (Grant NO. XDB34030301).

Appendix A: Basics of $B\bar{B}$ Production and related Polarization Observables

The total cross section for $e^+e^- \rightarrow B\bar{B}$ reaction reads as:

$$\sigma_B = \frac{4\pi\alpha_{\text{em}}^2\beta C(q^2)}{3q^2} \left[|G_M^B(q^2)|^2 + \frac{|G_E^B(q^2)|^2}{2\tau} \right] \quad (\text{A1})$$

in terms of the Sachs electric and magnetic form factors G_E and G_M . Here, α_{em} is the electromagnetic fine structure constant, β is the velocity of the final state nucleon or anti-nucleon in the e^+e^- center of mass system, $\tau = q^2/4m_B^2$ with $s = q^2$ and m_B being the invariant four-momentum transfer squared and the baryon mass, respectively, and $C(q^2)$ is the S-wave Sommerfeld-Gamow factor for the Coulomb correction [122]. In order to avoid the complication from phase space and Coulomb factor, later on we mainly discuss the effective form factor (EFF):

$$|G_{\text{eff}}^B| = \sqrt{\frac{2\tau|G_M^B(q^2)|^2 + |G_E^B(q^2)|^2}{2\tau + 1}} \quad (\text{A2})$$

which by definition could be extracted from the data of total cross section. The electro-magnetic ratio

$$R_B = \left| \frac{G_E^B(q^2)}{G_M^B(q^2)} \right| \quad (\text{A3})$$

could be determined by the data of different cross sections. Usually the alternative variable α_B are given by experiment of charmonium decaying to $B\bar{B}$:

$$\alpha_B = \frac{\tau - R_B^2}{\tau + R_B^2} \quad (\text{A4})$$

with τ defined in the peak mass of the charmonium state.

If the produced antinucleon is polarized when unpolarized electron beam is implemented, or if one of the colliding beam is longitudinally polarized then the antinucleon acquires x - and z -components of the polarization, which lie in the reaction plane, single-spin observables are defined as P_y and P_x , respectively.

$$P_y = \frac{\sin 2\theta}{\sqrt{\tau}D} \quad (\text{A5})$$

$$P_x = -\frac{2\sin\theta}{\sqrt{\tau}D} \text{Re}(G_M G_E^*) \text{Im}(G_M G_E^*) \quad (\text{A6})$$

with $D = (1 + \cos^2\theta)(|G_M|^2) + \frac{1}{\tau} \sin^2\theta |G_E|^2$. There are no more independent polarization variables.

In terms of isospin decomposition of nucleon-antinucleon production amplitudes, one arrives at:

$$\begin{aligned} \Re \left[\frac{G_M^{u+d}}{3} G_E^{u+d*} + G_M^{u-d} G_E^{u-d*} \right] &= -\frac{\sqrt{\tau_p} D_p P_x^p + \sqrt{\tau_n} D_n P_x^n}{\sin\theta} \\ \Re \left[\frac{G_M^{u+d}}{3} G_E^{u-d*} + G_M^{u-d} G_E^{u+d*} \right] &= -\frac{\sqrt{\tau_p} D_p P_x^p - \sqrt{\tau_n} D_n P_x^n}{\sin\theta} \\ \Im \left[\frac{G_M^{u+d}}{3} G_E^{u+d*} + G_M^{u-d} G_E^{u-d*} \right] &= \frac{\sqrt{\tau_p} D_p P_y^p + \sqrt{\tau_n} D_n P_y^n}{\sin\theta \cos\theta} \\ \Im \left[\frac{G_M^{u+d}}{3} G_E^{u-d*} + G_M^{u-d} G_E^{u+d*} \right] &= \frac{\sqrt{\tau_p} D_p P_y^p - \sqrt{\tau_n} D_n P_y^n}{\sin\theta \cos\theta} \end{aligned}$$

which probe the relative magnitudes and phases between $G_M^{u\pm d}$ and $G_E^{u\pm d}$.

In conclusion, four independent complex variables (2 isospin \times 2 electro-magnetic), e.g. seven independent real variables considering only relative phases are relevant, can be extracted from eight independent observables (total and differential cross sections, two polarization observables for proton and neutron) in each energy point.

[1] R. Hofstadter, *Rev. Mod. Phys.* **28**, 214 (1956).
 [2] X. Ji, F. Yuan, and Y. Zhao, *Nature Rev. Phys.* **3**, 27 (2021), arXiv:2009.01291 [hep-ph].

[3] R. Pohl *et al.*, *Nature* **466**, 213 (2010).
 [4] N. Bezginov, T. Valdez, M. Horbatsch, A. Marsman, A. C. Vutha, and E. A. Hessels, *Science* **365**, 1007

- (2019).
- [5] W. Xiong *et al.*, *Nature* **575**, 147 (2019).
- [6] I. Bombaci, *JPS Conf. Proc.* **17**, 101002 (2017), [arXiv:1601.05339 \[nucl-th\]](#).
- [7] A. Denig and G. Salme, *Prog. Part. Nucl. Phys.* **68**, 113 (2013), [arXiv:1210.4689 \[hep-ex\]](#).
- [8] S. Pacetti, R. Baldini Ferroli, and E. Tomasi-Gustafsson, *Phys. Rept.* **550-551**, 1 (2015).
- [9] M. A. Belushkin, H. W. Hammer, and U. G. Meissner, *Phys. Rev. C* **75**, 035202 (2007), [arXiv:hep-ph/0608337](#).
- [10] Y.-H. Lin, H.-W. Hammer, and U.-G. Meißner, *Phys. Rev. Lett.* **128**, 052002 (2022), [arXiv:2109.12961 \[hep-ph\]](#).
- [11] Y.-H. Lin, H.-W. Hammer, and U.-G. Meißner, *Eur. Phys. J. C* **82**, 1091 (2022), [arXiv:2208.14802 \[hep-ph\]](#).
- [12] F. Iachello, A. D. Jackson, and A. Lande, *Phys. Lett. B* **43**, 191 (1973).
- [13] G. Huang and R. B. Ferroli (BESIII), *Natl. Sci. Rev.* **8**, nwab187 (2021), [arXiv:2111.08425 \[hep-ex\]](#).
- [14] L. Xia, C. Rosner, Y. D. Wang, X. Zhou, F. E. Maas, R. B. Ferroli, H. Hu, and G. Huang, *Symmetry* **14**, 231 (2022), [arXiv:2111.13009 \[hep-ex\]](#).
- [15] D. Lin, A. Dbeyssi, and F. Maas, *Symmetry* **14**, 91 (2022).
- [16] P. Larin, X. Zhou, J. Hu, F. Maas, R. F. Baldini, H. Hu, and G. Huang, *Symmetry* **14**, 298 (2022).
- [17] X. Cao, V. Shklyar, and H. Lenske, *Phys. Rev. C* **88**, 055204 (2013), [arXiv:1303.2604 \[nucl-th\]](#).
- [18] M. Ablikim *et al.* (BESIII), *Phys. Rev. D* **100**, 032004 (2019), [arXiv:1904.10630 \[hep-ex\]](#).
- [19] M. Ablikim *et al.* (BESIII), (2021), [arXiv:2112.13219 \[hep-ex\]](#).
- [20] M. Ablikim *et al.* (BESIII), *Phys. Rev. D* **99**, 032001 (2019), [arXiv:1811.08742 \[hep-ex\]](#).
- [21] M. Ablikim *et al.* (BESIII), *Phys. Rev. Lett.* **124**, 112001 (2020), [arXiv:2001.04131 \[hep-ex\]](#).
- [22] M. Ablikim *et al.* (BESIII), *Phys. Rev. D* **105**, 032005 (2022), [arXiv:2112.15076 \[hep-ex\]](#).
- [23] A. Bianconi and E. Tomasi-Gustafsson, *Phys. Rev. Lett.* **114**, 232301 (2015), [arXiv:1503.02140 \[nucl-th\]](#).
- [24] A. Bianconi and E. Tomasi-Gustafsson, *Phys. Rev. C* **93**, 035201 (2016), [arXiv:1510.06338 \[nucl-th\]](#).
- [25] E. Tomasi-Gustafsson, A. Bianconi, and S. Pacetti, *Phys. Rev. C* **103**, 035203 (2021), [arXiv:2012.14656 \[hep-ph\]](#).
- [26] E. Tomasi-Gustafsson and S. Pacetti, *Phys. Rev. C* **106**, 035203 (2022).
- [27] J. P. B. C. de Melo, T. Frederico, E. Pace, S. Pisano, and G. Salme, *Phys. Lett. B* **671**, 153 (2009), [arXiv:0804.1511 \[hep-ph\]](#).
- [28] J. P. B. C. de Melo, T. Frederico, E. Pace, and G. Salme, *Phys. Rev. D* **73**, 074013 (2006), [arXiv:hep-ph/0508001](#).
- [29] I. T. Lorenz, H. W. Hammer, and U. G. Meißner, *Phys. Rev. D* **92**, 034018 (2015), [arXiv:1506.02282 \[hep-ph\]](#).
- [30] Q.-H. Yang, L.-Y. Dai, D. Guo, J. Haidenbauer, X.-W. Kang, and U.-G. Meißner, (2022), [arXiv:2206.01494 \[nucl-th\]](#).
- [31] R.-Q. Qian, Z.-W. Liu, X. Cao, and X. Liu, (2022), [arXiv:2211.11555 \[nucl-th\]](#).
- [32] X. Cao, J.-P. Dai, and H. Lenske, *Phys. Rev. D* **105**, L071503 (2022), [arXiv:2109.15132 \[hep-ph\]](#).
- [33] M. Ablikim *et al.* (BESIII), *Nature Phys.* **17**, 1200 (2021), [arXiv:2103.12486 \[hep-ex\]](#).
- [34] M. E. Biagini, E. Pasqualucci, and A. Rotondo, *Z. Phys. C* **52**, 631 (1991).
- [35] A. Antonelli *et al.*, *Nucl. Phys. B* **517**, 3 (1998).
- [36] M. N. Achasov *et al.*, *Phys. Rev. D* **90**, 112007 (2014), [arXiv:1410.3188 \[hep-ex\]](#).
- [37] V. P. Druzhinin and S. I. Serednyakov, *EPJ Web Conf.* **212**, 07007 (2019).
- [38] M. N. Achasov *et al.* (SND), *Eur. Phys. J. C* **82**, 761 (2022), [arXiv:2206.13047 \[hep-ex\]](#).
- [39] G. R. Farrar and D. R. Jackson, *Phys. Rev. Lett.* **35**, 1416 (1975).
- [40] V. L. Chernyak and I. R. Zhitnitsky, *Nucl. Phys. B* **246**, 52 (1984).
- [41] E. D. Bloom and F. J. Gilman, *Phys. Rev. Lett.* **25**, 1140 (1970).
- [42] D. Abrams *et al.* (Jefferson Lab Hall A Tritium), *Phys. Rev. Lett.* **128**, 132003 (2022), [arXiv:2104.05850 \[hep-ex\]](#).
- [43] E. P. Segarra, A. Schmidt, T. Kutz, D. W. Higinbotham, E. Piasetzky, M. Strikman, L. B. Weinstein, and O. Hen, *Phys. Rev. Lett.* **124**, 092002 (2020), [arXiv:1908.02223 \[nucl-th\]](#).
- [44] Z.-F. Cui, F. Gao, D. Binosi, L. Chang, C. D. Roberts, and S. M. Schmidt, *Chin. Phys. Lett.* **39**, 041401 (2022), [arXiv:2108.11493 \[hep-ph\]](#).
- [45] L. Chang, F. Gao, and C. D. Roberts, *Phys. Lett. B* **829**, 137078 (2022), [arXiv:2201.07870 \[hep-ph\]](#).
- [46] L.-M. Wang, S.-Q. Luo, and X. Liu, *Phys. Rev. D* **105**, 034011 (2022), [arXiv:2109.06617 \[hep-ph\]](#).
- [47] X. Liu, Q.-S. Zhou, and L.-M. Wang, *Phys. Rev. D* **106**, 094012 (2022), [arXiv:2209.11525 \[hep-ph\]](#).
- [48] J. R. Ellis and M. Karliner, *New J. Phys.* **4**, 18 (2002), [arXiv:hep-ph/0108259](#).
- [49] C. Alexandrou, S. Bacchio, M. Constantinou, J. Finkenrath, K. Hadjiyiannakou, K. Jansen, G. Koutsou, and A. Vaquero Aviles-Casco, *Phys. Rev. D* **100**, 014509 (2019), [arXiv:1812.10311 \[hep-lat\]](#).
- [50] M. Ablikim *et al.* (BESIII), (2022), [arXiv:2212.07071 \[hep-ex\]](#).
- [51] A. I. Milstein and S. G. Salnikov, (2022), [arXiv:2207.14020 \[hep-ph\]](#).
- [52] J. Haidenbauer, X. W. Kang, and U. G. Meißner, *Nucl. Phys. A* **929**, 102 (2014), [arXiv:1405.1628 \[nucl-th\]](#).
- [53] J. Haidenbauer, U.-G. Meißner, and L.-Y. Dai, *Phys. Rev. D* **103**, 014028 (2021), [arXiv:2011.06857 \[nucl-th\]](#).
- [54] G. Ramalho, M. T. Peña, and K. Tsushima, *Phys. Rev. D* **101**, 014014 (2020), [arXiv:1908.04864 \[hep-ph\]](#).
- [55] G. Ramalho, *Phys. Rev. D* **103**, 074018 (2021), [arXiv:2012.11710 \[hep-ph\]](#).
- [56] Z.-Y. Li, A.-X. Dai, and J.-J. Xie, *Chin. Phys. Lett.* **39**, 011201 (2022), [arXiv:2107.10499 \[hep-ph\]](#).
- [57] Z.-Y. Li and J.-J. Xie, *Commun. Theor. Phys.* **73**, 055201 (2021), [arXiv:2012.02379 \[hep-ph\]](#).
- [58] B. Yan, C. Chen, and J.-J. Xie, (2023), [arXiv:2301.00976 \[hep-ph\]](#).
- [59] B. Kubis and U. G. Meissner, *Eur. Phys. J. C* **18**, 747 (2001), [arXiv:hep-ph/0010283](#).
- [60] Y.-L. Liu and M.-Q. Huang, *Nucl. Phys. A* **821**, 80 (2009), [arXiv:0811.1812 \[hep-ph\]](#).
- [61] Y.-L. Liu and M.-Q. Huang, *Phys. Rev. D* **79**, 114031 (2009), [arXiv:0906.1935 \[hep-ph\]](#).
- [62] S. Xu, C. Mondal, J. Lan, X. Zhao, Y. Li, and J. P. Vary (BLFQ), *Phys. Rev. D* **104**, 094036 (2021), [arXiv:2108.03909 \[hep-ph\]](#).

- [63] C. Mondal, S. Xu, J. Lan, X. Zhao, Y. Li, D. Chakrabarti, and J. P. Vary, *Phys. Rev. D* **102**, 016008 (2020), arXiv:1911.10913 [hep-ph].
- [64] T. Peng, Z. Zhu, S. Xu, X. Liu, C. Mondal, X. Zhao, and J. P. Vary (BLFQ), *Phys. Rev. D* **106**, 114040 (2022), arXiv:2208.00355 [hep-ph].
- [65] H.-W. Lin and K. Orginos, *Phys. Rev. D* **79**, 074507 (2009), arXiv:0812.4456 [hep-lat].
- [66] M. Yang and P. Wang, *Phys. Rev. D* **105**, 016006 (2022), arXiv:2110.13089 [hep-ph].
- [67] A.-X. Dai, Z.-Y. Li, L. Chang, and J.-J. Xie, *Chin. Phys. C* **46**, 073104 (2022), arXiv:2112.06264 [hep-ph].
- [68] A. Bianconi and E. Tomasi-Gustafsson, *Phys. Rev. C* **105**, 065206 (2022), arXiv:2204.05197 [hep-ph].
- [69] R. Baldini, S. Pacetti, A. Zallo, and A. Zichichi, *Eur. Phys. J. A* **39**, 315 (2009), arXiv:0711.1725 [hep-ph].
- [70] J. M. Alarcón, A. N. Hiller Blin, M. J. Vicente Vacas, and C. Weiss, *Nucl. Phys. A* **964**, 18 (2017), arXiv:1703.04534 [hep-ph].
- [71] M. Ablikim *et al.* (BESIII), *Phys. Lett. B* **814**, 136110 (2021), arXiv:2009.01404 [hep-ex].
- [72] M. Ablikim *et al.* (BESIII), *Phys. Lett. B* **831**, 137187 (2022), arXiv:2110.04510 [hep-ex].
- [73] B. Aubert *et al.* (BaBar), *Phys. Rev. D* **76**, 092006 (2007), arXiv:0709.1988 [hep-ex].
- [74] (2022), arXiv:2210.16761 [hep-ex].
- [75] V. L. Chernyak, A. A. Ogloblin, and I. R. Zhitnitsky, *Yad. Fiz.* **48**, 1410 (1988).
- [76] X. Zhou, L. Yan, R. B. Ferroli, and G. Huang, *Symmetry* **14**, 144 (2022).
- [77] M. Ablikim *et al.* (BESIII), *Phys. Lett. B* **831**, 137187 (2022), arXiv:2110.04510 [hep-ex].
- [78] M. Ablikim *et al.* (BESIII), *Phys. Rev. D* **104**, L091104 (2021), arXiv:2108.02410 [hep-ex].
- [79] M. Ablikim *et al.* (BESIII), (2023), arXiv:2303.07629 [hep-ex].
- [80] M. Ablikim *et al.* (BESIII), *Phys. Rev. D* **103**, 012005 (2021), arXiv:2010.08320 [hep-ex].
- [81] M. Ablikim *et al.* (BESIII), *Phys. Lett. B* **820**, 136557 (2021), arXiv:2105.14657 [hep-ex].
- [82] M. Ablikim *et al.* (BESIII), *Phys. Rev. Lett.* **124**, 032002 (2020), arXiv:1910.04921 [hep-ex].
- [83] X. Wang and G. Huang, *Symmetry* **14**, 65 (2022).
- [84] R. L. Workman *et al.* (Particle Data Group), *PTEP* **2022**, 083C01 (2022).
- [85] M. Ablikim *et al.* (BESIII), *Phys. Rev. D* **86**, 032014 (2012), arXiv:1205.1036 [hep-ex].
- [86] M. Ablikim *et al.* (BESIII), *Phys. Lett. B* **770**, 217 (2017), arXiv:1612.08664 [hep-ex].
- [87] M. Ablikim *et al.* (BESIII), *Nature* **606**, 64 (2022), arXiv:2105.11155 [hep-ex].
- [88] M. Ablikim *et al.* (BESIII), *Phys. Rev. D* **95**, 052003 (2017), arXiv:1701.07191 [hep-ex].
- [89] M. Ablikim *et al.* (BESIII), *Phys. Rev. Lett.* **125**, 052004 (2020), arXiv:2004.07701 [hep-ex].
- [90] M. Ablikim *et al.* (BESIII), *Nature Phys.* **15**, 631 (2019), arXiv:1808.08917 [hep-ex].
- [91] M. Ablikim *et al.* (BESIII), *Phys. Rev. D* **98**, 032006 (2018), arXiv:1803.02039 [hep-ex].
- [92] M. Ablikim *et al.* (BESIII), *Phys. Rev. D* **106**, L091101 (2022), arXiv:2206.10900 [hep-ex].
- [93] M. Ablikim *et al.* (BESIII), *JHEP* **12**, 016 (2022), arXiv:2209.14564 [hep-ex].
- [94] S.-M. Wu, J.-J. Wu, and B.-S. Zou, *Phys. Rev. D* **104**, 054018 (2021), arXiv:2104.09908 [hep-ph].
- [95] M. Claudson, S. L. Glashow, and M. B. Wise, *Phys. Rev. D* **25**, 1345 (1982).
- [96] S. Dobbs, A. Tomaradze, T. Xiao, K. K. Seth, and G. Bonvicini, *Phys. Lett. B* **739**, 90 (2014), arXiv:1410.8356 [hep-ex].
- [97] X. H. Mo and J. Y. Zhang, *Phys. Lett. B* **826**, 136927 (2022), arXiv:2111.15045 [hep-ph].
- [98] R. Baldini Ferroli, A. Mangoni, S. Pacetti, and K. Zhu, *Phys. Lett. B* **799**, 135041 (2019), arXiv:1905.01069 [hep-ph].
- [99] Y. P. Guo and C. Z. Yuan, *Phys. Rev. D* **105**, 114001 (2022), arXiv:2203.00244 [hep-ph].
- [100] L.-G. Xia, *Phys. Lett. B* **756**, 77 (2016), arXiv:1508.02039 [hep-ph].
- [101] N. Kivel, *Eur. Phys. J. A* **58**, 26 (2022), arXiv:2109.05847 [hep-ph].
- [102] N. Kivel, *Eur. Phys. J. A* **58**, 138 (2022), arXiv:2203.00377 [hep-ph].
- [103] N. Kivel, (2022), arXiv:2211.13603 [hep-ph].
- [104] N. Kivel, *Eur. Phys. J. A* **56**, 64 (2020), [Erratum: *Eur.Phys.J.A* 57, 271 (2021)], arXiv:1910.02850 [hep-ph].
- [105] R. Wang, X. Cao, and X. Chen, *Phys. Lett. B* **747**, 321 (2015), arXiv:1411.0534 [hep-ph].
- [106] Y. M. Bystritskiy, *Phys. Rev. D* **103**, 116029 (2021), arXiv:2104.01483 [hep-ph].
- [107] Y. M. Bystritskiy and A. I. Ahmadov, *Phys. Rev. D* **105**, 116012 (2022), arXiv:2204.08956 [hep-ph].
- [108] R.-Q. Qian, Q. Huang, and X. Liu, *Phys. Lett. B* **833**, 137292 (2022), arXiv:2111.13821 [hep-ph].
- [109] J. P. Lees *et al.* (BaBar), *Phys. Rev. D* **88**, 072009 (2013), arXiv:1308.1795 [hep-ex].
- [110] J. P. Lees *et al.* (BaBar), *Phys. Rev. D* **87**, 092005 (2013), arXiv:1302.0055 [hep-ex].
- [111] M. Ablikim *et al.* (BESIII), *Phys. Lett. B* **735**, 101 (2014), arXiv:1403.6011 [hep-ex].
- [112] M. Ablikim *et al.* (BESIII), *Phys. Rev. D* **91**, 112004 (2015), arXiv:1504.02680 [hep-ex].
- [113] D. Djukanovic, K. Ottnad, J. Wilhelm, and H. Wittig, *Phys. Rev. Lett.* **123**, 212001 (2019), arXiv:1903.12566 [hep-lat].
- [114] B. Kubis and R. Lewis, *Phys. Rev. C* **74**, 015204 (2006), arXiv:nucl-th/0605006.
- [115] J.-Z. Wang, L.-M. Wang, X. Liu, and T. Matsuki, *Phys. Rev. D* **104**, 054045 (2021), arXiv:2106.14582 [hep-ph].
- [116] Q.-S. Zhou, J.-Z. Wang, X. Liu, and T. Matsuki, *Phys. Rev. D* **105**, 074035 (2022), arXiv:2201.06393 [hep-ph].
- [117] C.-Q. Pang, *Phys. Rev. D* **99**, 074015 (2019), arXiv:1902.02206 [hep-ph].
- [118] C.-Q. Pang, Y.-R. Wang, J.-F. Hu, T.-J. Zhang, and X. Liu, *Phys. Rev. D* **101**, 074022 (2020), arXiv:1910.12408 [hep-ph].
- [119] Y.-R. Wang, T.-Y. Li, Z.-Y. Fang, H. Chen, and C.-Q. Pang, *Phys. Rev. D* **106**, 114024 (2022), arXiv:2208.10329 [hep-ph].
- [120] C.-Q. Pang, B. Wang, X. Liu, and T. Matsuki, *Phys. Rev. D* **92**, 014012 (2015), arXiv:1505.04105 [hep-ph].
- [121] M. Achasov *et al.*, (2023), arXiv:2303.15790 [hep-ex].
- [122] A. D. Sakharov, *Zh. Eksp. Teor. Fiz.* **18**, 631 (1948).